


Potassium octatitanate fibers induce persistent lung and pleural injury and are possibly carcinogenic in male Fischer 344 rats

Mohamed Abdelgied^{1,2,3} | Ahmed M. El-Gazzar^{1,2,4} | David B. Alexander¹  | William T. Alexander¹ | Takamasa Numano¹ | Masaaki Iigou¹ | Aya Naiki-Ito² | Hirotugu Takase⁵ | Khaled Abbas Abdou³ | Akihiko Hirose⁶ | Yuhji Taquahashi⁷ | Jun Kanno⁸ | Hiroyuki Tsuda¹ | Satoru Takahashi²

¹Nanotoxicology Project, Nagoya City University, Nagoya, Japan

²Department of Experimental Pathology and Tumor Biology, Nagoya City University Graduate School of Medical Sciences, Nagoya, Japan

³Department of Forensic Medicine and Toxicology, Faculty of Veterinary Medicine, Beni-Suef University, Beni-Suef, Egypt

⁴Department of Forensic Medicine and Toxicology, Faculty of Veterinary Medicine, Alexandria University, Alexandria, Egypt

⁵Core Laboratory, Nagoya City University Graduate School of Medical Sciences, Nagoya, Japan

⁶Division of Risk Assessment, National Institute of Health Sciences, Tokyo, Japan

⁷Division of Cellular and Molecular Toxicology, National Institute of Health Sciences, Tokyo, Japan

⁸Japan Industrial Safety and Health Association, Japan Bioassay Research Center, Kanagawa, Japan

Correspondence

Hiroyuki Tsuda and David B. Alexander,
Nanotoxicology Project, Nagoya City
University, Nagoya, Japan.
Emails: htsuda@phar.nagoya-cu.ac.jp (H.T.),
dalexand@phar.nagoya-cu.ac.jp (D.B.A.)

Funding information

Egyptian Cultural Affairs and Missions
Sector (Grant/Award Number: na), Health
and Labour Sciences Research Grants of
Japan (Grant/Award Number: "H22-kagaku-
ippan-005, H25-kagaku-ippan-004, H28-
ka"), 5th Term Long-Range Research
Initiative (2017) by Japan Chemical
Industry Association (Grant/Award Number:
na).

Potassium octatitanate fibers ($K_2O \cdot 8TiO_2$, POT fibers) are widely used as an alternative to asbestos. We investigated the pulmonary and pleural toxicity of POT fibers with reference to 2 non-fibrous titanium dioxide nanoparticles ($nTiO_2$), photoreactive anatase ($a-nTiO_2$) and inert rutile ($r-nTiO_2$). Ten-week-old male F344 rats were given 0.5 mL of 250 $\mu\text{g/mL}$ suspensions of POT fibers, $a-nTiO_2$, or $r-nTiO_2$, 8 times (1 mg/rat) over a 15-day period by trans-tracheal intrapulmonary spraying (TIPS). Rats were killed at 6 hours and at 4 weeks after the last TIPS dose. Alveolar macrophages were significantly increased in all treatment groups at 6 hours and at 4 weeks. At week 4, $a-nTiO_2$ and $r-nTiO_2$ were largely cleared from the lung whereas a major fraction of POT fibers were not cleared. In the bronchoalveolar lavage, alkaline phosphatase activity was elevated in all treatment groups, and lactate dehydrogenase (LDH) activity was elevated in the $a-nTiO_2$ and POT groups. In lung tissue, oxidative stress index and proliferating cell nuclear antigen (PCNA) index were elevated in the $a-nTiO_2$ and POT groups, and there was a significant elevation in C-C motif chemokine ligand 2 (CCL2) mRNA and protein in the POT group. In pleural cavity lavage, total protein was elevated in all 3 treatment groups, and LDH activity was elevated in the $a-nTiO_2$ and POT groups. Importantly, the PCNA index of the visceral mesothelium was increased in the POT group. Overall, POT fibers had greater biopersistence, induced higher expression of CCL2, and provoked a stronger tissue response than $a-nTiO_2$ or $r-nTiO_2$.

This is an open access article under the terms of the Creative Commons Attribution-NonCommercial License, which permits use, distribution and reproduction in any medium, provided the original work is properly cited and is not used for commercial purposes.

© 2018 The Authors. *Cancer Science* published by John Wiley & Sons Australia, Ltd on behalf of Japanese Cancer Association.

KEYWORDS

inhalation toxicity, potassium octatitanate fiber, rat, titanium dioxide nanoparticle, trans-tracheal intrapulmonary spraying

1 | INTRODUCTION

Because of its high tensile strength, chemical stability, and heat-resistance, potassium octatitanate (POT) is commonly used as an alternative to asbestos. POT fibers have a long needle-like shape, similar to asbestos, and are not broken down in the body.¹ Thus, the fiber pathogenicity paradigm² identifies these fibers as potential carcinogens.

The carcinogenicity of POT fibers was confirmed by an initial study that gave POT fibers directly to the pleural surface of Osborne-Mendel rats and a later study that gave POT fibers by i.p. injection.³⁻⁵ Two recent studies infused POT fibers directly into the pleural cavity of mice and rats: one study followed the treated animals for 52 and 65 weeks⁶ and the other study followed the treated animals for 52 weeks.⁷ Although none of the treated animals had developed mesothelioma by the time the study was terminated, all mice and rats treated with POT fibers exhibited pleural thickening. Inhalation studies that followed exposed animals for up to 2 years were mostly negative.⁸⁻¹² Overall, these studies indicate that POT fibers are carcinogenic, but that a high amount of POT fibers in prolonged contact with susceptible tissue is required for induction of malignant neoplasia. They also suggest that inhalation of POT fibers is not carcinogenic in rats and that low level exposure may not be carcinogenic in humans.⁸ See Doc. S1 for a brief discussion of the studies cited here.

Thus, the physical characteristics of POT fibers suggest high carcinogenic potential, but the experimental evidence indicates low carcinogenic potential. A variety of factors could account for this discrepancy: (i) the fiber pathogenicity paradigm may not apply to POT fibers, possibly because of the chemical make-up of the fibers. (ii) The relatively low sensitivity of inhalation studies using rats may be a factor in the negative results of the inhalation studies (see p. 100 Bignon et al¹³; the low sensitivity of rat inhalation studies is also noted by Mohr et al¹⁴). (iii) If the fibers are not well dispersed, this will result in lower than expected levels of particles with small enough aerodynamic diameters to penetrate beyond the ciliated airways.

To resolve these problems and determine whether further experimentation on the carcinogenicity of POT fibers is warranted, we conducted a short-term experiment comparing the intensity of early indicators of possible carcinogenicity in rats given POT fibers or non-fibrous titanium dioxide nanoparticles (nTiO₂). We used two types of nTiO₂, photoreactive anatase (a-nTiO₂) and inert rutile (r-nTiO₂): a-nTiO₂ is a weak carcinogen in the lung that induces neoplastic development when high doses are given.¹⁵ The major component of these materials is titanium but the

shapes (granular particles, short rods, and long needle-like-shaped fibers) are different. All 3 particle types were dispersed by the Taquann method to ensure maximum dispersion and given by trans-tracheal intrapulmonary spraying (TIPS) on account of the higher sensitivity of TIPS administration compared to exposure by inhalation. Therefore, if the fiber pathogenicity paradigm does not hold for POT fibers, as suggested by the inhalation studies cited above, then giving equal amounts of well-dispersed POT fibers and a-nTiO₂ and r-nTiO₂ using TIPS should have similar effects, or the POT fibers may induce a weaker response than the nTiO₂ particles because of the much lower number of particles. If, however, the fiber pathogenicity paradigm does apply to POT fibers, then these fibers would be expected to be more biopersistent and induce a stronger response than the nTiO₂ particles, and further experimentation on the carcinogenicity of POT fibers would be warranted.

2 | MATERIALS AND METHODS

2.1 | Preparation of particle suspension

Potassium octatitanate fibers and a-nTiO₂ and r-nTiO₂ particles were supplied by Dr A. Hirose (one of the authors). All 3 particles were dispersed by the Taquann method¹⁶ to generate dispersed single fibers/particles, and stored in tert-butyl alcohol. Shortly before administration, frozen t-butyl alcohol was removed using an Eyla Freeze Dryer (FDU-2110; Tokyo Rikakikai Co., Ltd, Tokyo, Japan), and POT fibers were suspended in saline containing 0.5% Pluronic F-68 (PF68; Sigma-Aldrich, St Louis, MO, USA) at 250 µg/mL and a-nTiO₂ and r-nTiO₂ particles were suspended in saline at 250 µg/mL. After suspension in vehicle, test materials were sonicated for 2 minutes 4 times at 3000 rpm using a polytron PT 1600E bench top homogenizer (Kinematika AG, Lattau, Switzerland). To minimize aggregation, the suspensions were sonicated for 30 minutes immediately prior to administration.

2.2 | Characterization of particles in suspension

After sonication, 20 µL of each test material suspension was placed on a carbon-supported 200 mesh micro grid membrane (200-Cu; Nisshin EM Co., Ltd, Tokyo, Japan); the shape of the nanoparticles was imaged by transmission electron microscopy (JEOL Co. Ltd, Tokyo, Japan), and the photos were analyzed by NIH image analyzer software (NIH, Bethesda, MD, USA). Over 1000 particles of each type of material were measured. Element analysis was done using a scanning electron microscope with an X-ray microanalyzer (ADEX,

Tokyo, Japan) after loading small aliquots of each test material directly after freeze-drying on carbon conductive double-faced adhesive tabs (Nisshin EM Co., Ltd).

2.3 | Animals

Nine-week-old male F344 rats were purchased from Charles River Japan Inc. (Kanagawa, Japan). The animals were housed in the animal center of Nagoya City University Medical School, maintained on a 12-hour light-dark cycle, and received oriental MF basal diet (Oriental Yeast Co., Tokyo, Japan) and water ad libitum. The experimental protocol was approved by the Animal Care and Use Committee of Nagoya City University Medical School, and the research was conducted according to the Guidelines for the Care

and Use of Laboratory Animals of Nagoya City University Medical School.

2.4 | Experimental design and tissue sample collection

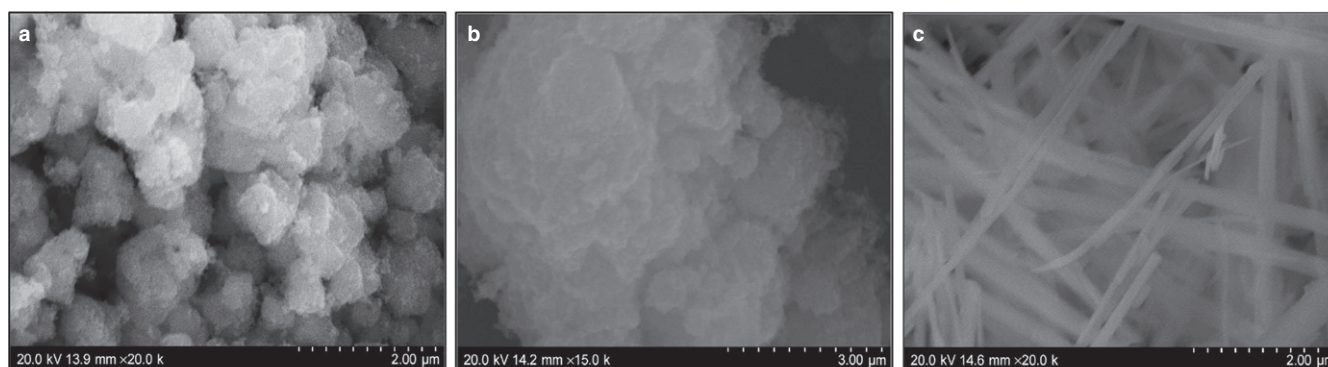
After acclimatization for 1 week, 96 rats were divided into 6 groups of 16 animals each: group 1, without treatment; group 2, vehicle (saline); group 3, vehicle (saline plus 0.5% PF68); group 4, a-nTiO₂ (250 µg/mL); group 5, r-nTiO₂ (250 µg/mL); and group 6, POT fibers (250 µg/mL). Vehicle (0.5 mL) and test material suspensions (0.5 mL; 125 µg of test material) were given to the animals by TIPS using a microsyringe (series IA-1B Intratracheal Aerosolizer; Penn-Century, Philadelphia, PA, USA) under 3% isoflurane anesthesia as described

TABLE 1 Sequences of the actin, CCL2, CCL3, and CCL4 primers used in real-time PCR

Gene	Forward	Reverse
Actin	GGGAAATCGTGCCTGACA	AGGAAGGAAGGCTGGAAGA
CCL2	GATCTCTCTTCCACCACACTAT	GTTCTCCAGCCGACTCATTG
CCL3	CGACTGCCTGCTGCTTCT	TTCCTTGCTGCTCTAATCTCA
CCL4	GTGTCTGCCTTCTCTCTCC	AGGCTGCTGGTCTCATAGT

CCL, C-C motif chemokine ligand.

(A)



(B)

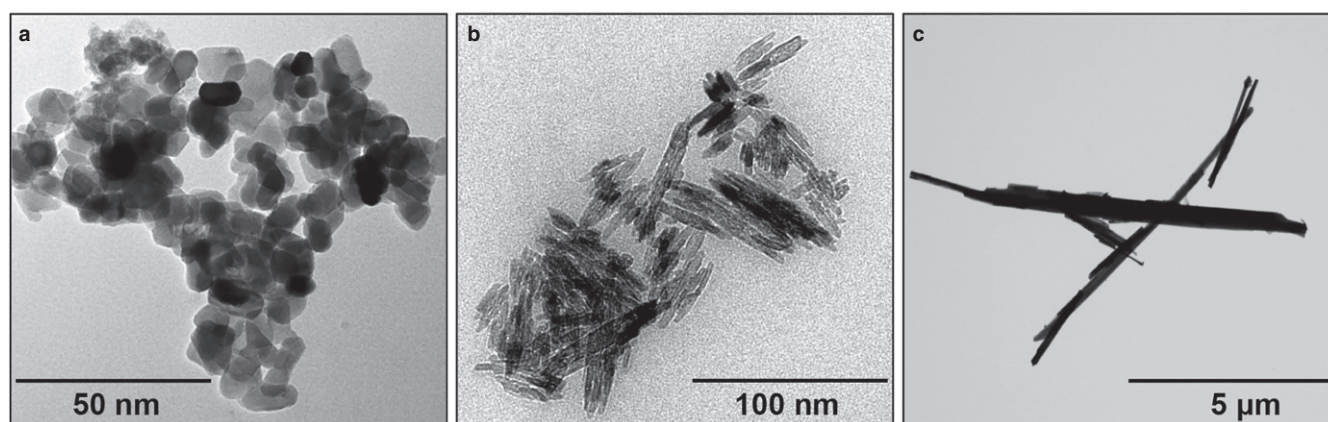


FIGURE 1 Characterization of test materials in suspension. A, Scanning electron microscope images and B, transmission electron microscopy images of a, photoreactive anatase (a-nTiO₂), b, inert rutile (r-nTiO₂), and c, potassium octatitanate (POT) fibers

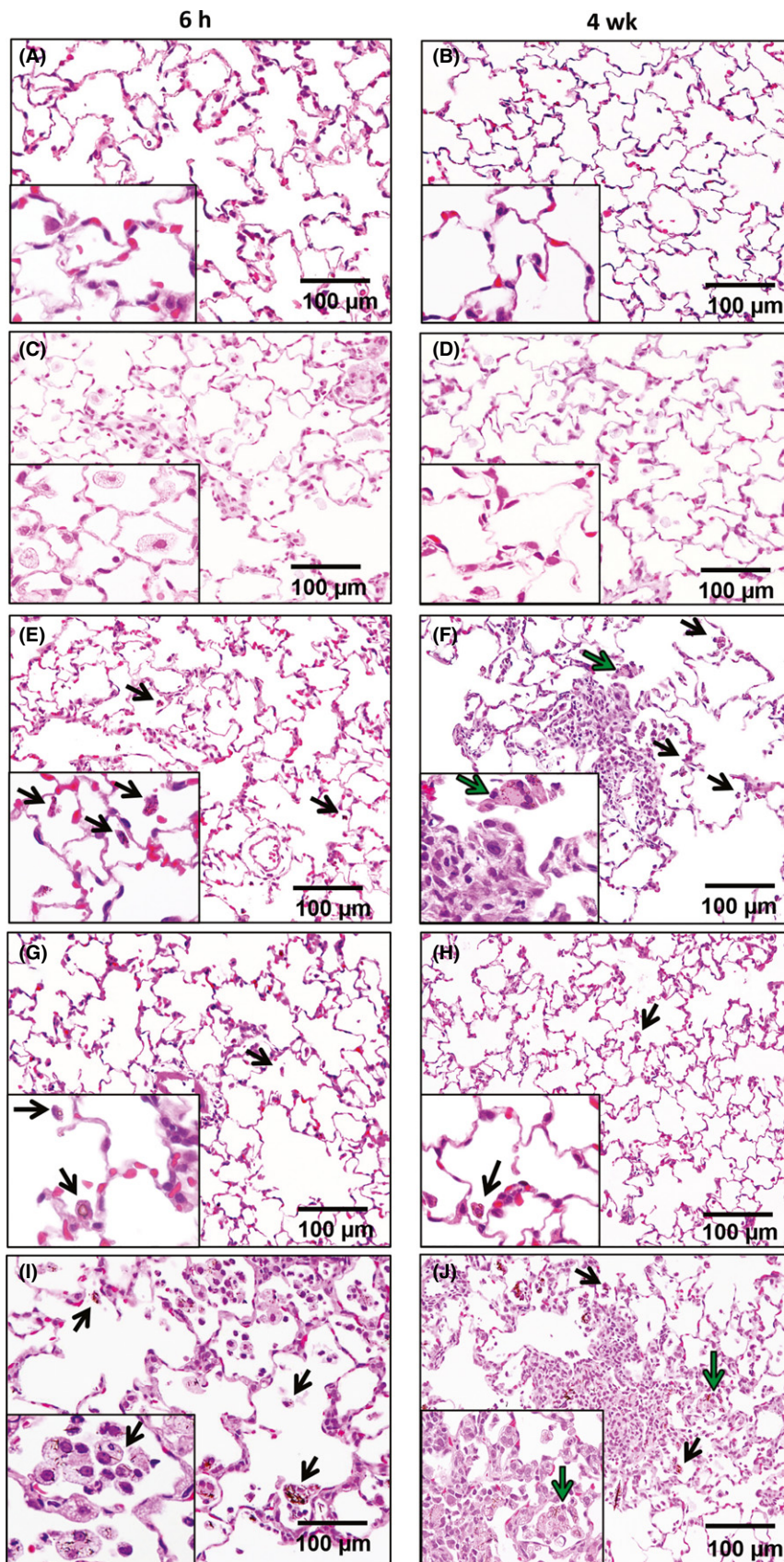


FIGURE 2 Histological observation of lung tissue at 6 h and at 4 wks after the final trans-tracheal intrapulmonary spraying dose of A, B, saline, C, D, saline + PF68, E, F, photoreactive anatase (a-nTiO₂), G, H, inert rutile (r-nTiO₂), and I, J, potassium octatitanate (POT) fibers. Black arrows indicate alveolar macrophages phagocytizing test materials, and green arrows indicate multinucleated giant cells

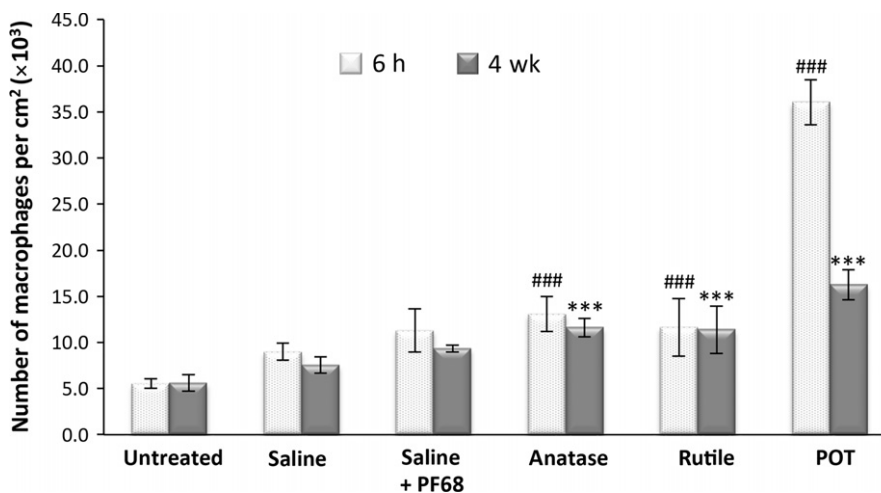


FIGURE 3 Alveolar macrophage counts per cm² of lung tissue. ###*P* < .001 vs vehicle (photoreactive anatase [a-nTiO₂] and inert rutile [r-nTiO₂] vs saline; potassium octatitanate [POT] vs saline + PF68) at 6 h, and ****P* < .001 vs vehicle (a-nTiO₂ and r-nTiO₂ vs saline; POT vs saline + PF68) 4 wks after the final trans-tracheal intrapulmonary spraying dose

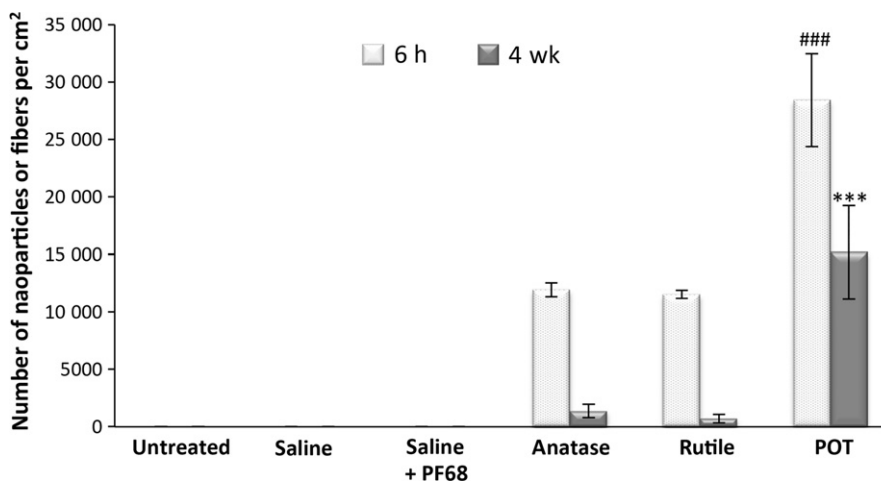


FIGURE 4 Nanoparticle/fiber count per cm² of lung tissue. ###*P* < .001 vs photoreactive anatase (a-nTiO₂) and inert rutile (r-nTiO₂) at 6 h and ****P* < .001 vs a-nTiO₂ and r-nTiO₂ 4 wks after the final trans-tracheal intrapulmonary spraying dose. POT, potassium octatitanate

previously.¹⁷ Rats were treated once every other day over a 15-day period (8 doses; total of 1 mg of test material). At 6 hours and at 4 weeks after the last dose, 8 rats from each group were killed by exsanguination from the abdominal aorta under deep anesthesia. Serum samples were stored at −80°C.

At 6 hours, the lung was excised and the right lung lobes were cut into pieces and immediately frozen at −80°C for biochemical analysis, and the left lung was fixed in 4% paraformaldehyde solution adjusted to pH 7.3 and processed for immunohistochemical, light microscopic, and electron microscopic examination. At 4 weeks, the left lung was used for collection of bronchoalveolar lavage fluid and right lung lobes were divided into 2 parts: the first part was immediately frozen at −80°C and used for biochemical analysis, and the second part, as well as the trachea and mediastinal lymph nodes, was fixed in buffered 4% paraformaldehyde solution and processed for immunohistochemical, light microscopic, and electron microscopic examination.

2.5 | Light microscopy, polarized light microscopy, and electron microscopy

Lung, trachea, and mediastinal lymph nodes were processed for H&E staining. Identification of the dosed materials in the tissue cells and alveolar macrophages was made by polarized light microscopy (PLM; Olympus, Tokyo, Japan). For high-magnification viewing, slides were immersed in xylene to remove the cover glass, then immersed in 100% ethanol, air-dried and coated with platinum, and viewed by SEM (Field Emission Scanning Electronic Microscope; Hitachi High Technologies, Tokyo, Japan) at 5–10 kV. For ultrafine viewing of the localization of the dosed materials in the lung, the area in the paraffin block corresponding to the H&E slide was cut out, deparaffinized, and embedded in epoxy resin and processed for transmission electron microscopy (TEM) equipped with an X-ray element microanalyzer (EDAX, Tokyo, Japan).

For PCNA staining, sections were incubated with PBS containing 5% BSA and 5% goat serum for at least 1 hour, then

incubated with anti-PCNA (Cell Signaling Technology, Danvers, MA, USA) diluted 1:2000 in PBS containing 1% BSA and 1% goat serum overnight at 4°C, then incubated with secondary antibody (Nichirei Biosciences, Tokyo, Japan), visualized with DAB (Nichirei Biosciences), and counterstained with hematoxylin. In each lung specimen, more than 1000 pulmonary epithelial cells and more than 500 visceral pleural mesothelial cells were counted blindly in random fields. All nuclei showing brown staining of more than half of the nucleus were considered to be positive.

2.6 | Collection and biochemical analysis of pleural lavage fluid

RPMI 1640 (10 mL) was injected into the pleural cavity through the left side of the diaphragm, the thoracic wall was gently massaged, and the lavage fluid was aspirated through the right side of the diaphragm. The pleural lavage fluid (PLF) was centrifuged at 500 g at 4°C for 5 minutes and the supernatant was stored at -80°C until use (the cell pellets were used for preparation of pleural lavage cell pellets, described below). Lactate dehydrogenase (LDH) activity was measured using an LDH activity assay kit (Sigma-Aldrich) and total protein concentration was measured using the BCA Protein Assay Kit (Pierce Biotech, Rockford, IL, USA).

2.7 | Pleural lavage cell pellet preparation

Cell pellets from 2 animals in the same group were combined and suspended in 5 mL of 1% RBC lysis buffer (BioLegend Inc., San Diego, CA, USA), then centrifuged at 500 g at 4°C for 5 minutes. The supernatant was discarded, and the cell pellet was fixed by suspension in buffered 4% paraformaldehyde at 4°C overnight, then centrifuged at 500 g at 4°C for 5 minutes. The pellet was washed with saline and centrifuged at 900 g at 4°C for 5 minutes. Sodium alginate (0.5 mL of 1%) and 20 μ L of 1 M CaCl_2 was added to the pellet, and the pellet was stored in 80% EtOH prior to embedding in paraffin and processing for histopathology.

2.8 | Collection and biochemical analysis of bronchoalveolar lavage fluid

The thoracic cavity was opened and the right bronchus was tied just below the bifurcation and the left lung was cannulated using a 25 G canula through the trachea. Bronchoalveolar lavage was carried out 3 times with 10 mL of sterile ice-cold Mg^{++} - and Ca^{++} -free PBS plus 0.6 mM EDTA. Bronchoalveolar lavage fluid (BALF) was centrifuged at 500 g at 4°C for 5 minutes and the supernatant was stored at -80°C until use. Lactate dehydrogenase (LDH) activity was measured using an LDH activity assay kit (Sigma-Aldrich), alkaline phosphatase

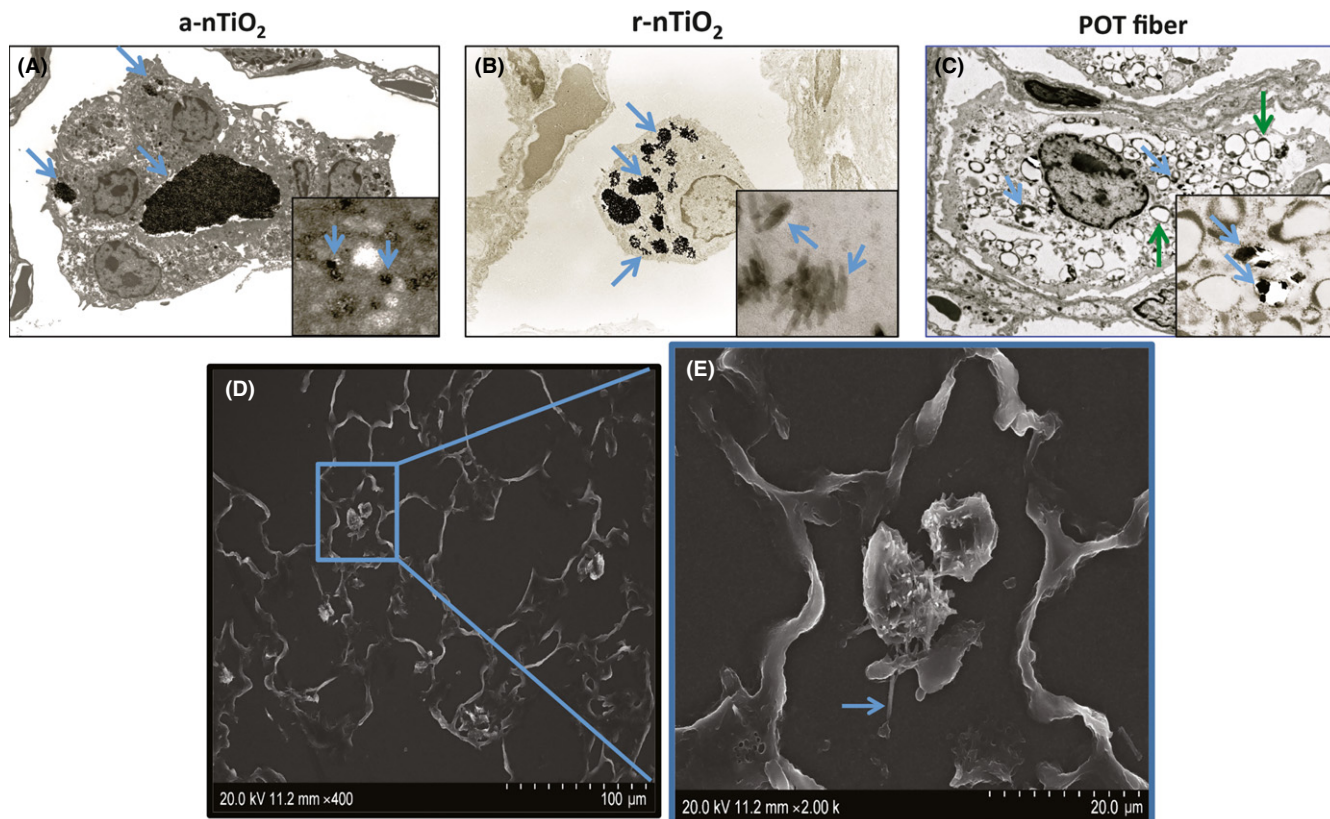


FIGURE 5 Transmission electron microscopy (TEM) and scanning electronic microscopy (SEM) of alveolar macrophages. (A-C) TEM images of the 3 test materials (blue arrows) and cytoplasmic vacuoles in the macrophages phagocytosing POT fibers (green arrows). (D, E) SEM images of alveolar macrophages phagocytosing a POT fiber (arrow). a-nTiO₂, photoreactive anatase; POT, potassium octatitanate; r-nTiO₂, inert rutile

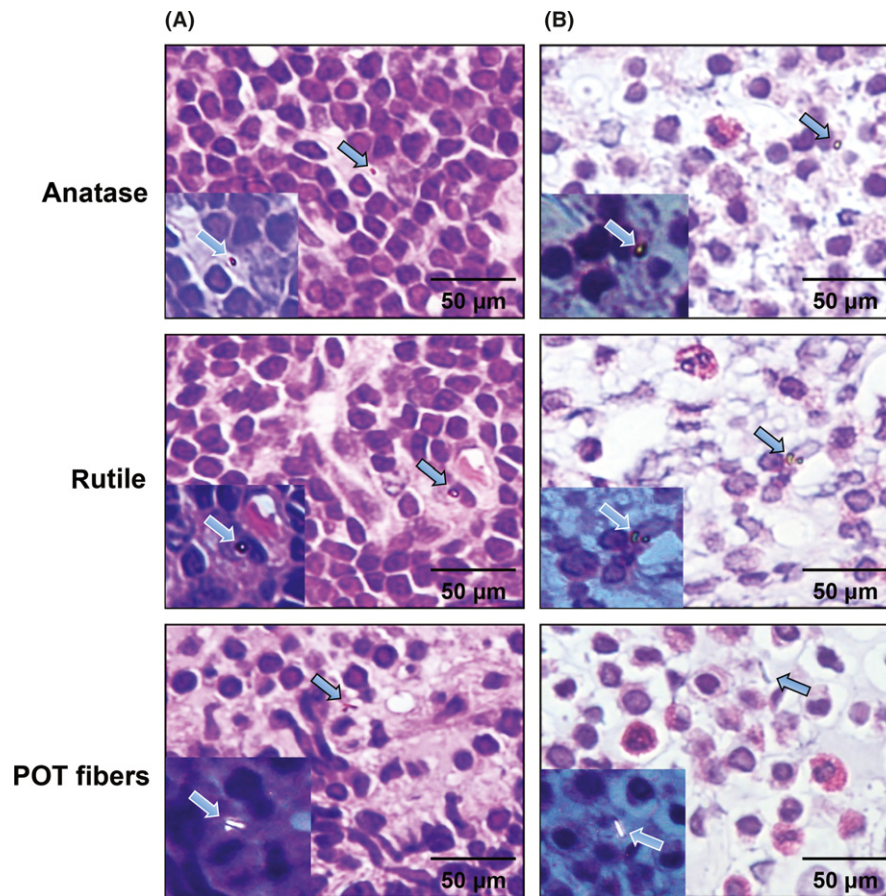


FIGURE 6 Translocation of the test materials. A, All 3 test materials were detected in the mediastinal lymph nodes (arrows). B, The 3 test materials were also present in the pleural cavity lavage cell pellets (arrows). POT, potassium octatitanate

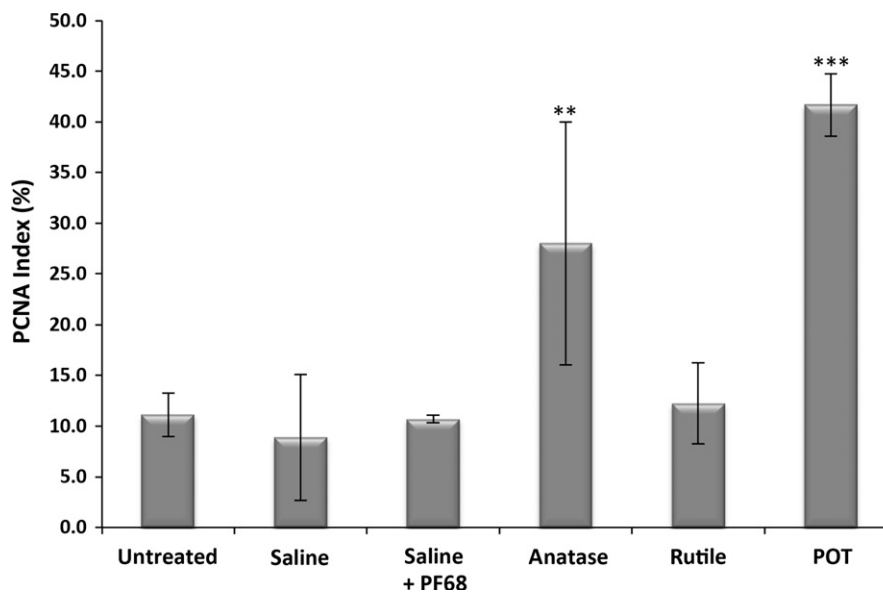


FIGURE 7 Proliferating cell nuclear antigen (PCNA) staining of lung tissue. PCNA index expressed as the percentage of PCNA-positive cells to the total number of pulmonary cells per slide. ** $P < .01$ and *** $P < .001$ vs vehicle (photoreactive anatase [α - nTiO_2] vs saline; potassium octatitanate [POT] vs saline + PF68) 4 wks after the final trans-tracheal intrapulmonary spraying dose

(ALP) activity was measured using an ALP enzyme activity assay kit (Wako Chemicals Co., Ltd, Tokyo, Japan), and total protein concentration was measured using the BCA Protein Assay Kit (Pierce Biotech).

2.9 | RNA isolation, cDNA synthesis, and RT-PCR analysis of gene expression

Pieces of the right lungs (50–100 mg) were thawed, rinsed 3 times with ice-cold PBS, homogenized using a disposable BioMasher II (Nippi, Inc., Tokyo, Japan) in 1 mL Trizol reagent (Life Technologies Corp., Carlsbad, CA, USA), and total RNA was isolated. Concentration and quality (integrity) of the RNA was measured using the Agilent 2100 Bioanalyzer chip system (Agilent Technologies, Inc., Santa Clara, CA, USA) with an Agilent RNA 6000 Nano kit (Agilent Technologies, Inc.). RNA integrity numbers of all samples were higher than 7. Total RNA (500 ng) was used for RT-PCR using the SuperScript™ III system (Invitrogen, Carlsbad, CA, USA). Real-time PCR was carried out with

Power SYBR Green PCR Master Mix (Applied Biosystems, Carlsbad, CA, USA) in MicroAmp Optical 96-well Reaction Plates (Applied Biosystems) using an Applied Biosystems 7300 Real-Time PCR System. Cycling parameters were 2 minutes at 50°C and 10 minutes at 95°C followed by 40 cycles of 15 seconds at 95°C and 60 seconds at 60°C. Each reaction in the 96-well plates was carried out in triplicate and results from 3 independent 96-well plates were used for analysis. Target genes were normalized to actin using the $2^{-\Delta\Delta CT}$ method¹⁸ with actin and target gene reactions carried out in the same 96-well plates. Primers were designed using Primer Premier 6.11 software (Premier Biosoft International, Palo Alto, CA, USA) and purchased from Sigma-Aldrich. Primers are listed in Table 1.

2.10 | Biochemical analysis and ELISA for lung tissues

Frozen right lung tissue samples (approximately 100 mg) were thawed and rinsed 3 times with ice-cold PBS and homogenized in 1 mL tissue

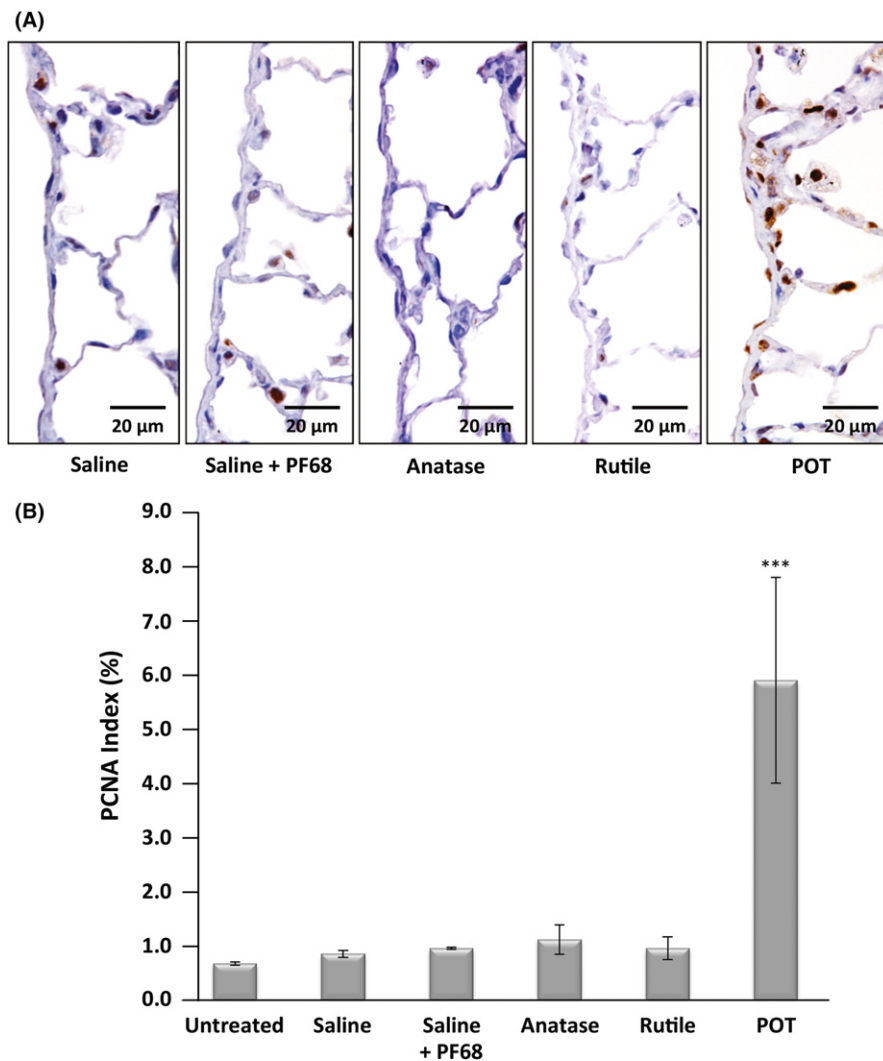


FIGURE 8 Visceral mesothelial cell proliferation. A, Proliferating cell nuclear antigen (PCNA) staining of visceral mesothelial cells. B, PCNA index expressed as the percentage of PCNA-positive cells to the total number of visceral mesothelial cells per slide. *** $P < .001$ vs vehicle (saline + PF68) 4 wks after the final trans-tracheal intrapulmonary spraying dose. POT, potassium octatitanate

protein extraction reagent (Thermo Scientific, Rockford, IL, USA) containing 1% (v/v) protease inhibitor cocktail (Sigma-Aldrich). The homogenates were centrifuged at 9000 *g* for 5 minutes at 4°C. Protein content of the supernatant was measured using the BCA Protein Assay Kit (Pierce Biotech). Level of CCL2 in the supernatant was measured using a Mouse/Rat CCL2 ELISA Kit (R&D systems, Inc., Minneapolis, MN, USA) according to the manufacturer's instructions.

Total oxidant status (TOS) and total antioxidant capacity (TAC) levels were measured using total antioxidant status and total oxidant status kits (Rel Assay Diagnostics, Gaziantep, Turkey) according to the manufacturer's instructions. TOS units are $\mu\text{mol H}_2\text{O}_2$ equivalents per gram of tissue, TAC units are $\mu\text{mol Trolox}$ equivalents per gram of tissue, and oxidative stress index (OSI) was calculated as $\text{OSI} = \text{TOS}/\text{TAC}$.¹⁹⁻²¹

2.11 | Statistical analysis

All data are expressed as means \pm SD. Data were analyzed for homogeneity of variance using Levene's test. Statistical significance was analyzed by one-way ANOVA when the variance was homogenous and Welch's *t* test when the variance was not homogenous using SPSS software version 23 (IBM, Armonk, New York, USA). A value of $P < .05$ was considered to be significant.

3 | RESULTS

3.1 | Characterization of titanium compounds

SEM images of the 3 test materials show that both a-nTiO₂ and r-nTiO₂ form agglomerates and POT fibers are straight needle-like shapes (Figure 1A). TEM images show that individual a-nTiO₂ nanoparticles are tetragonal in shape; individual r-nTiO₂ nanoparticles have short, thick rod-like shapes; and individual POT fibers have straight needle-like shapes (Figure 1B). Mean diameter of a-nTiO₂ was 6.02 ± 3.40 nm, mean length and width of r-nTiO₂ was 50.02 ± 8.24 nm and 14.35 ± 4.63 nm, respectively, and mean length and width of the POT fibers was 6.06 ± 1.53 μm and 305 ± 69 nm, respectively. Dimensions of all 3 test materials were evenly distributed around their means (Figure S1).

Element analysis showed that both a-nTiO₂ and r-nTiO₂ nanoparticles were composed of 60% titanium and 40% oxygen, and POT fibers were composed of 52.1% titanium, 37.0% oxygen, and 10.8% potassium. This is in agreement with the molecular ratio of each element in the tested materials.

3.2 | Alveolar macrophage and fiber/particle count in the lung

At 6 hours, alveolar macrophages with vacuolated cytoplasm were present in the treated animals and also in the vehicle controls (Figure 2). At 4 weeks, inflammation in the lungs of the vehicle control rats had subsided and macrophages with

vacuolated cytoplasm were no longer present (Figure 2B,D). At both 6 hours and at 4 weeks, alveolar macrophages with internalized test materials were present in all 3 treatment groups (Figure 2E-J). Macrophages with POT fibers appeared to be somewhat larger in size with vacuolar changes in the cytoplasm (Figure 2I). There was scattered granuloma formation in the lungs of both a-nTiO₂- and POT-treated rats (Figure 2F,J). Slight fibrotic changes of the alveolar wall in areas of granulomatous inflammation were observed.

At both 6 hours and at 4 weeks, there was a significant increase in the number of alveolar macrophages in all 3 treatment groups (Figure 3; Table S1). At 4 weeks, both a-nTiO₂ and r-nTiO₂ particles were largely cleared from the lung; in contrast, a large proportion of POT fibers was still present in the lung 4 weeks after the end of

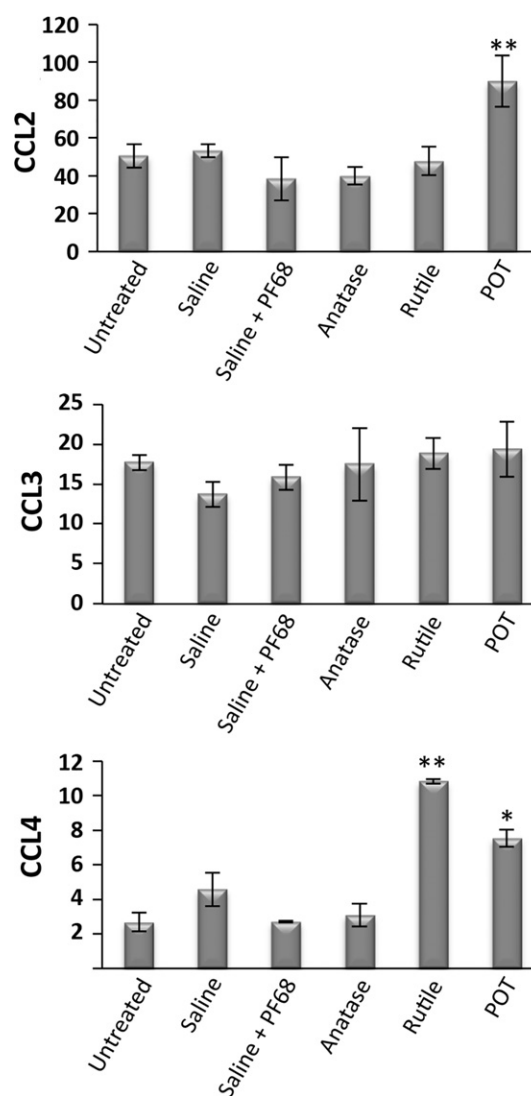


FIGURE 9 Proinflammatory cytokine gene expression in lung tissue. Graphs show RNA expression of the target cytokines relative to actin. * $P < .05$ and ** $P < .01$ vs vehicle (inert rutile [r-nTiO₂] vs saline; potassium octatitanate [POT] vs saline + PF68) 4 wks after the final trans-tracheal intrapulmonary spraying dose. CCL, C-C motif chemokine ligand

TIPS dosage (Figure 4; Table S1). TEM observation showed a-nTiO₂ and r-nTiO₂ completely engulfed in the cytoplasm of alveolar macrophages without any distortion of cell shape (Figure 5A,B) and a few large aggregates of anatase and rutile TiO₂ particles surrounded by several macrophages (Figure 5A). In contrast, alveolar macrophages engulfing POT fibers showed vacuolar changes and cellular degeneration (Figure 5C). SEM showed POT fibers penetrating alveolar macrophages, indicating frustrated phagocytosis was occurring (Figure 5D,E).

All 3 test materials were detected in the mediastinal lymph nodes (Figure 6A), and in pleural cavity lavage cell pellets (Figure 6B). In the pleural lavage cell pellet, both a-nTiO₂ and r-nTiO₂ were completely phagocytized inside cells whereas most POT fibers appeared to be free; the cell population was a mixture of macrophages, lymphocytes, eosinophils, and neutrophils.

3.3 | Pulmonary and visceral mesothelial cell proliferation

At 4 weeks, there were significant increases in the PCNA labeling indices of lung alveolar cells in the a-nTiO₂ (28.0 ± 12.0) and POT (41.7 ± 3.1) treatment groups compared with their vehicle control groups, 8.9 ± 6.2 and 10.7 ± 0.4, respectively, ($P < .001$) (Figure 7; Table S2). PCNA labeling index of visceral mesothelial cells was also significantly increased in the POT treatment group (5.9 ± 1.9) compared to its vehicle control group (0.96 ± 0.02) ($P < .001$) (Figures 8 and S2; Table S2). We also found an area of hyperplasia in the visceral pleura of a POT-treated rat (Figure S3).

3.4 | Expression of proinflammatory cytokines

At 4 weeks, there was a significant increase ($P < .01$) in CCL2 and CCL4, but not in CCL3, RNA expression in the lungs of the POT-treated rats compared to its vehicle control, and a significant

increase ($P < .05$) in CCL4 expression in the lungs of the r-nTiO₂ treatment group (Figure 9; Table S3).

As the RNA expression level of CCL2 was approximately 10-fold higher than that of CCL4 and as CCL2 is a primary chemoattractant of macrophages and is overexpressed across a broad range of tumor types,^{22,23} we measured the protein levels of CCL2 in lung tissue. At 4 weeks, there was a significant increase ($P < .001$) in CCL2 protein expression in the lungs of the POT (31.92 ± 8.28)-treated animals compared to the vehicle controls (17.38 ± 1.79) (Figure 10; Table S4).

3.5 | Total oxidant status, total antioxidant capacity, and oxidative stress index

At 4 weeks, there was a slight, but significant, elevation of TOS and OSI in the lungs of the a-nTiO₂-treated rats and a more marked elevation of TOS and OSI in the lungs of POT-treated rats compared to their vehicle controls (Figure 11; Table S5). There was no difference in TAC in any of the 3 treatment groups compared to their vehicle controls.

3.6 | Bronchial and pleural lavage supernatants

At 4 weeks, LDH activity in BALF was significantly higher in the a-nTiO₂ (2132.88 ± 781.94)- and POT (2243.05 ± 515.44)-treated rats compared to their vehicle controls (927.94 ± 369.06 and 794.06 ± 246.86), and ALP activity in BALF was significantly higher in all 3 treatment groups (a-nTiO₂ 455.49 ± 33.10; r-nTiO₂ 245.37 ± 10.44; and POT 526.58 ± 139.09) compared to their vehicle controls (161.73 ± 19.31 and 139.34 ± 113.08) (Figure 12; Table S6). There was no significant change in total protein concentration in BALF among the groups (Table S6).

At 4 weeks, LDH activity in pleural cavity lavage was significantly higher in the a-nTiO₂ (1815.12 ± 611.04)- and POT

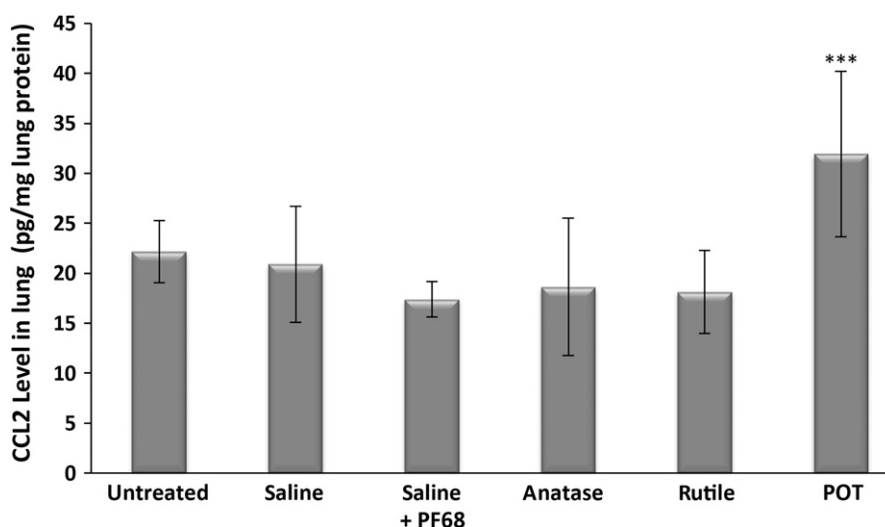


FIGURE 10 C-C motif chemokine ligand 2 (CCL2) protein expression in lung tissue. *** $P < .001$ vs vehicle (saline + PF68) 4 wks after the final trans-tracheal intrapulmonary spraying dose. POT, potassium octatitanate

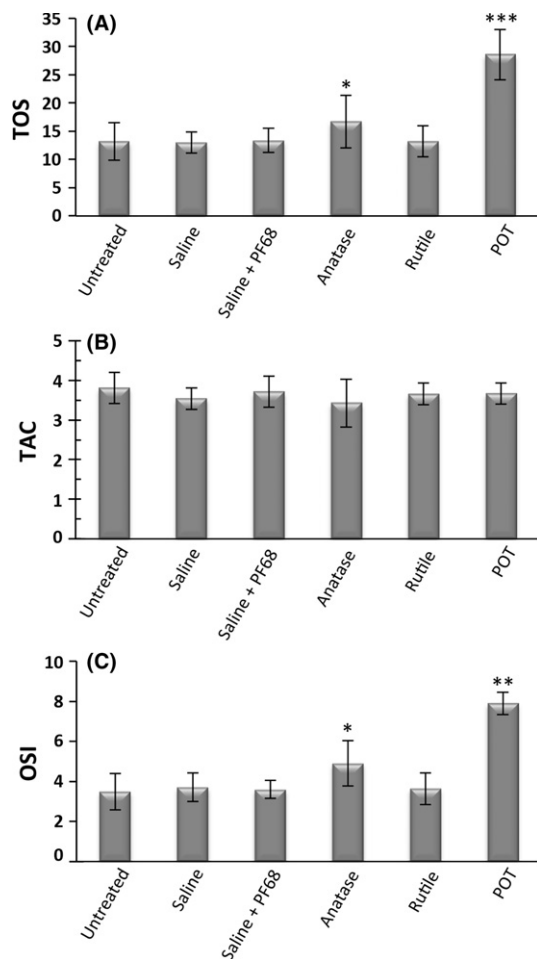


FIGURE 11 Total oxidant status (TOS), total antioxidant capacity (TAC), and oxidative stress index (OSI) in lung tissue. A, TOS is expressed as $\mu\text{mol H}_2\text{O}_2$ equivalents per gram of tissue. B, TAC is expressed as $\mu\text{mol Trolox}$ equivalents per gram of tissue. C, OSI is expressed as the ratio of TOS to TAC. * $P < .05$, ** $P < .01$, and *** $P < .001$ vs vehicle (photoreactive anatase [a- nTiO_2] vs saline; potassium octatitanate [POT] vs saline + PF68) 4 wks after the final trans-tracheal intrapulmonary spraying dose

(1876.58 ± 729.54)-treated rats compared to their vehicle controls (1076.35 ± 455.17 and 918.20 ± 329.32), and there was a significant increase in total protein concentration in all 3 treatment groups (a- nTiO_2 289.83 ± 140.56 ; r- nTiO_2 160.32 ± 27.56 ; and POT 218.59 ± 109.46) compared to their vehicle controls (89.24 ± 69.05 and 106.92 ± 33.25) (Figure 13; Table S7).

4 | DISCUSSION

The physical characteristics of POT fibers and their ability to induce malignant mesothelioma when placed in direct contact with the mesothelial lining suggest high carcinogenic potential;³⁻⁵ however, experimental evidence from inhalation studies suggests inhaled POT fibers elicit little or no carcinogenic response⁸⁻¹² (please see Doc. S1 for a brief discussion of the fiber pathogenicity paradigm and

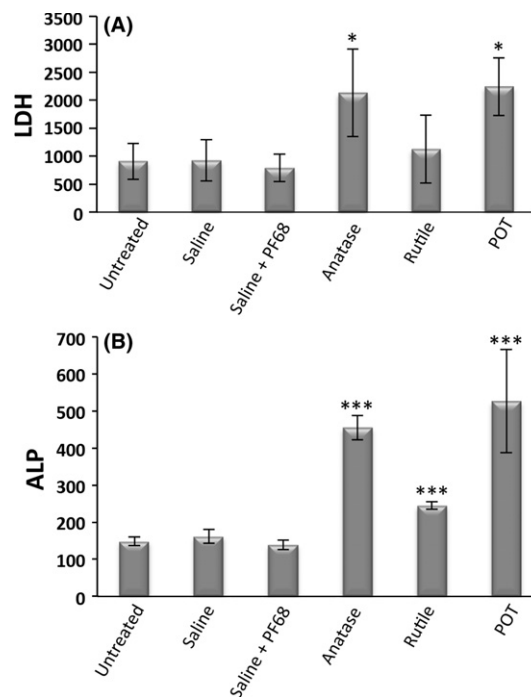


FIGURE 12 Biochemical analysis of bronchoalveolar lavage fluid. A, Lactate dehydrogenase (LDH) enzyme activity, measured as micro-units/L and B, alkaline phosphatase (ALP) enzyme concentration, measured as units/L. * $P < .05$ and *** $P < .001$ vs vehicle (photoreactive anatase [a- nTiO_2] and inert rutile [r- nTiO_2] vs saline; potassium octatitanate [POT] vs saline + PF68) 4 wks after the final trans-tracheal intrapulmonary spraying dose

long-term studies on POT fibers). Factors such as the chemical make-up of POT fibers, how well the tested POT fibers were dispersed, and the sensitivity of the animal model to respirable carcinogens could play a role in this seeming contradiction. In the present short-term study, we gave well-dispersed POT fibers ($\text{K}_2\text{O} \cdot 8\text{TiO}_2$; straight needle-like shape), anatase titanium dioxide nanoparticles (a- nTiO_2 ; non-fibrous tetragonal shape), and rutile titanium dioxide nanoparticles (r- nTiO_2 ; non-fibrous short rod-like shape) to rats using TIPS, a method conferring higher sensitivity to respirable carcinogens than inhalation exposure. The results of this study indicate that POT fibers are more biopersistent, induce a greater degree of pulmonary and pleural injury, and elicit more intense early indicators of possible carcinogenicity than a- nTiO_2 or r- nTiO_2 .

Biopersistence of particles in the lung that have been deposited beyond the ciliated airways depends on clearance of the particle by macrophages and the stability of the particle in the biological milieu of the lung. Long fibers that are not stable can be fragmented into shorter fibers and, consequently, unstable fibers will be cleared from the lung.^{24,25} POT fibers are biologically stable and have been recovered from rat lung 12 months after short-term inhalation exposure with no change in their surface or diameter.¹ Therefore, macrophage-mediated clearance is believed to be the main mechanism of clearance of POT fibers from the lung.¹ Macrophage

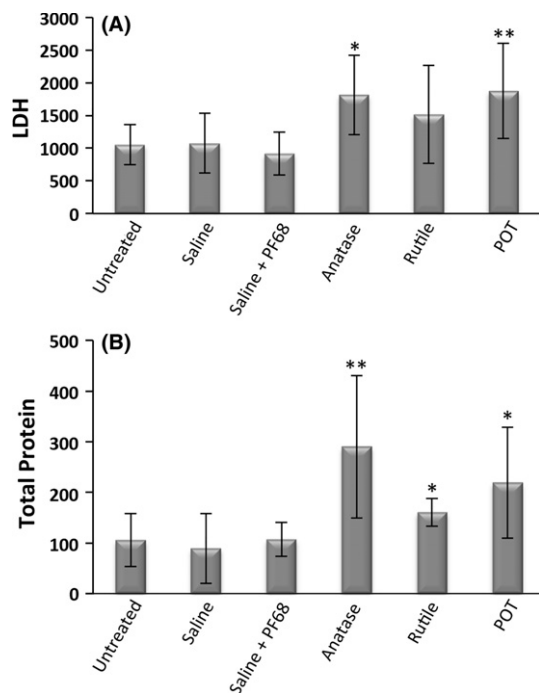


FIGURE 13 Biochemical analysis of pleural cavity lavage fluid. A, Lactate dehydrogenase (LDH) enzyme activity, measured as micro-units/L and B, total protein concentration ($\mu\text{g/mL}$). * $P < .05$ and ** $P < .01$ vs vehicle (photoreactive anatase [a-nTiO₂] and inert rutile [r-nTiO₂] vs saline; potassium octatitanate [POT] vs saline + PF68) 4 wks after the final trans-tracheal intrapulmonary spraying dose

clearance of particles deposited in the lower airways is affected by the shape and size of the particle. Phagocytosis of silver nanowires $>5 \mu\text{m}$ in length has been shown to impede the movement of macrophages.²⁶ A large percentage of POT fibers, but not a-nTiO₂ or r-nTiO₂ particles, would be expected to inhibit macrophage clearance of fibers out of the lower airway (Figure S1). Another factor is that attempted phagocytosis of fibers that exceed the phagocytic capacity of the macrophage leads to frustrated phagocytosis (Figure 5E) and results in production of chemotaxins that retain macrophages, preventing their migration to the mucociliary escalator.²⁷ In agreement with this data, in the present study, a significant fraction of POT fibers were not cleared from the lung whereas a-nTiO₂ and r-nTiO₂ particles were almost completely cleared from the lungs of treated rats.

Although a-nTiO₂ and r-nTiO₂ particles were largely cleared from the lungs at week 4, macrophages actively phagocytosing these particles, as well as POT fibers, were observed in the lungs of treated rats at week 4 (Figure 2). TiO₂ particle-laden macrophages, including macrophages in which the particles are completely engulfed, are expected to generate reactive oxygen species (ROS) and other inflammatory mediators²⁸ (see also figure 5 in Hamilton et al., 2009)²⁹ and cause tissue damage. In our study, all 3 materials caused an increase in ALP levels (an indicator of type II epithelial cell toxicity) and a-nTiO₂ and POT fibers caused increases in LDH

levels (an indicator of general toxicity) and oxidative stress in lung tissue. Overall, POT fibers were more toxic than a-nTiO₂ or r-nTiO₂, and r-nTiO₂ was the least toxic of the 3 materials. PCNA index of the lung tissue followed the pattern of toxicity (compare Figure 7 with Figures 11 and 12), indicating repair of damaged tissue.

Cytokine analysis of the lung tissue indicated a highly significant upregulation of CCL2 in the POT treatment group 4 weeks after the end of TIPS dosage. CCL2 is a potent chemotaxin and its expression can lead to the recruitment of macrophages, monocytes, and monocytic myeloid-derived suppressor cells (M-MDSC),^{30,31} and this is associated with tumor development.³¹⁻³³

All 3 test materials were detected in the mediastinal lymph nodes and pleural cell pellets (Figure 6) in agreement with the tenet that particles and fibers deposited in the lung, if not cleared by mucociliary clearance or alveolar macrophages, can be transported into the lymphatic system and hence into the pleural space.³⁴⁻³⁶ As in the lung, particle-laden macrophages are expected to provoke tissue damage and, in our study, all 3 materials caused an increase in the protein concentration of the PLF (an indicator of general toxicity) and POT- and a-nTiO₂-treated rats also had elevated LDH levels. Importantly, however, only POT fibers caused an increase in the PCNA index in the visceral pleura. It is also notable that 1 of the POT-treated rats had an area of hyperplasia in the visceral pleura.

POT fibers have greater biopersistence, provoked a stronger tissue response, and induced higher expression of CCL2 than either a-nTiO₂ or r-nTiO₂. We propose the following mechanism to explain possible carcinogenicity of POT fibers in the lung. Biopersistence of POT fibers results in persistent generation of ROS and reactive nitrogen species (RNS) and other inflammatory mediators by macrophages attempting to clear POT fibers out of the lung and pleural cavity. The resultant tissue damage caused by this inflammatory response and the damage caused by the fibers themselves results in a tissue repair response. Consequently, the generation of DNA-damaging oxidants in the presence of cells replicating in response to tissue damage creates a milieu in which DNA-damaging ROS and RNS can damage the DNA of dividing cells, allowing replication of damaged DNA before it is repaired, resulting in fixation of mutations in the DNA of the daughter cells. (Please see Doc. S2 for a detailed discussion of how this mechanism is proposed to operate in asbestos-induction of malignant mesothelioma.)

The biopersistence of POT fibers and the subsequent response to these fibers coupled with production of CCL2 and the ensuing infiltration of potentially tumor-promoting myeloid cells suggest that POT fibers may be carcinogenic in the lung and pleura of rats. The hyperplastic lesion found in 1 of the POT fiber-treated rats is also an indicator of possible POT fiber-mediated carcinogenesis, as mesothelial cell hyperplasia is exceedingly rare in rats. Based on these results, we are conducting a long-term study to further investigate the possible carcinogenicity of POT fibers.

ACKNOWLEDGMENTS

This work was supported by Health and Labour Sciences Research Grants by the Ministry of Health, Labour and Welfare Japan (Grant Number: "H27-kagaku-shitei-004," "H25-kagaku-ippan-004," "H28-kagaku-ippan-004"), the 5th Term Long-Range Research Initiative (2017) by Japan Chemical Industry Association, and Egyptian Cultural Affairs and Missions Sector.

CONFLICT OF INTEREST

Authors declare no conflicts of interest for this article.

ORCID

David B. Alexander  <http://orcid.org/0000-0002-9017-3639>

REFERENCES

- Yamato H, Morimoto Y, Tsuda T, et al. Clearance of inhaled potassium Octatitanate Whisker from rat lungs. *J Occup Health*. 2002;44:34-39.
- Donaldson K, Murphy F, Schinwald A, Duffin R, Poland CA. Identifying the pulmonary hazard of high aspect ratio nanoparticles to enable their safety-by-design. *Nanomedicine (Lond)*. 2011;6:143-156.
- Adachi S, Kawamura K, Takemoto K. A trial on the quantitative risk assessment of man-made mineral fibers by the rat intraperitoneal administration assay using the JFM standard fibrous samples. *Ind Health*. 2001;39:168-174.
- Stanton MF, Layard M. The carcinogenicity of fibrous minerals. In: Gravatt CC, LaFleur PD, Heinrich KFJ, eds. *Workshop on Asbestos: Definitions and Measurement Methods*, vol. 506. Washington, DC: National Measurement Laboratory National Bureau of Standards; 1978:143-151.
- Stanton MF, Layard M, Tegeris A, et al. Relation of particle dimension to carcinogenicity in amphibole asbestoses and other fibrous minerals. *J Natl Cancer Inst*. 1981;67:965-975.
- Yokohira M, Hashimoto N, Nakagawa T, et al. Long-term chronic toxicity and mesothelial cell reactions induced by potassium octatitanate fibers (TISMO) in the left thoracic cavity in A/J female mice. *Int J Toxicol*. 2015;34:325-335.
- Yokohira M, Nakano-Narusawa Y, Yamakawa K, et al. Chronic mesothelial reaction and toxicity of potassium octatitanate fibers in the pleural cavity in mice and F344 rats. *Cancer Sci*. 2016;107:1047-1054.
- Ikegami T, Tanaka A, Taniguchi M, et al. Chronic inhalation toxicity and carcinogenicity study on potassium octatitanate fibers (TISMO) in rats. *Inhal Toxicol*. 2004;16:291-310.
- Lee KP, Barras CE, Griffith FD, Waritz RS. Pulmonary response and transmigration of inorganic fibers by inhalation exposure. *Am J Pathol*. 1981;102:314-323.
- Lee KP, Barras CE, Griffith FD, Waritz RS, Lapin CA. Comparative pulmonary responses to inhaled inorganic fibers with asbestos and fiberglass. *Environ Res*. 1981;24:167-191.
- Oyabu T, Yamato H, Ogami A, et al. The effect of lung burden on biopersistence and pulmonary effects in rats exposed to potassium octatitanate whiskers by inhalation. *J Occup Health*. 2004;46:382-390.
- Yamato H, Oyabu T, Ogami A, et al. Pulmonary effects and clearance after long-term inhalation of potassium octatitanate whiskers in rats. *Inhal Toxicol*. 2003;15:1421-1434.
- Bignon J, Brochard P, Brown R, et al. Assessment of the toxicity of man-made fibres. A final report of a workshop held in Paris, France 3-4 February 1994. *Ann Occup Hyg*. 1995;39:89-106.
- Mohr U, Ernst H, Roller M, Pott F. Pulmonary tumor types induced in Wistar rats of the so-called "19-dust study". *Exp Toxicol Pathol*. 2006;58:13-20.
- Drummond G, Bevan R, Harrison P. A comparison of the results from intra-pleural and intra-peritoneal studies with those from inhalation and intratracheal tests for the assessment of pulmonary responses to inhalable dusts and fibres. *Regul Toxicol Pharmacol*. 2016;81:89-105.
- Taquahashi Y, Ogawa Y, Takagi A, Tsuji M, Morita K, Kanno J. Improved dispersion method of multi-wall carbon nanotube for inhalation toxicity studies of experimental animals. *J Toxicol Sci*. 2013;38:619-628.
- Xu J, Futakuchi M, Shimizu H, et al. Multi-walled carbon nanotubes translocate into the pleural cavity and induce visceral mesothelial proliferation in rats. *Cancer Sci*. 2012;103:2045-2050.
- Livak KJ, Schmittgen TD. Analysis of relative gene expression data using real-time quantitative PCR and the 2(-DeltaDeltaC(T)) Method. *Methods*. 2001;25:402-408.
- Erel O. A novel automated direct measurement method for total antioxidant capacity using a new generation, more stable ABTS radical cation. *Clin Biochem*. 2004;37:277-285.
- Erel O. A new automated colorimetric method for measuring total oxidant status. *Clin Biochem*. 2005;38:1103-1111.
- Harma M, Harma M, Erel O. Increased oxidative stress in patients with hydatidiform mole. *Swiss Med Wkly*. 2003;133:563-566.
- Zhang J, Lu Y, Pienta KJ. Multiple roles of chemokine (C-C motif) ligand 2 in promoting prostate cancer growth. *J Natl Cancer Inst*. 2010;102:522-528.
- Majety M, Runza V, Lehmann C, Hoves S, Ries CH. A drug development perspective on targeting tumor-associated myeloid cells. *FEBS J*. 2018;285:763-776.
- Boulanger G, Andujar P, Pairon JC, et al. Quantification of short and long asbestos fibers to assess asbestos exposure: a review of fiber size toxicity. *Environ Health*. 2014;13:59.
- Donaldson K, Schinwald A, Murphy F, et al. The biologically effective dose in inhalation nanotoxicology. *Acc Chem Res*. 2013;46:723-732.
- Schinwald A, Chernova T, Donaldson K. Use of silver nanowires to determine thresholds for fibre length-dependent pulmonary inflammation and inhibition of macrophage migration in vitro. *Part Fibre Toxicol*. 2012;9:47.
- Donaldson K, Poland CA, Murphy FA, MacFarlane M, Chernova T, Schinwald A. Pulmonary toxicity of carbon nanotubes and asbestos - similarities and differences. *Adv Drug Deliv Rev*. 2013;65:2078-2086.
- Brown DM, Donaldson K, Borm PJ, et al. Calcium and ROS-mediated activation of transcription factors and TNF-alpha cytokine gene expression in macrophages exposed to ultrafine particles. *Am J Physiol Lung Cell Mol Physiol*. 2004;286:L344-L353.
- Hamilton RF, Wu N, Porter D, Buford M, Wolfarth M, Holian A. Particle length-dependent titanium dioxide nanomaterials toxicity and bioactivity. *Part Fibre Toxicol*. 2009;6:35.
- Deshmane SL, Kremlev S, Amini S, Sawaya BE. Monocyte chemoattractant protein-1 (MCP-1): an overview. *J Interferon Cytokine Res*. 2009;29:313-326.
- Huang B, Lei Z, Zhao J, et al. CCL2/CCR2 pathway mediates recruitment of myeloid suppressor cells to cancers. *Cancer Lett*. 2007;252:86-92.
- Solinas G, Germano G, Mantovani A, Allavena P. Tumor-associated macrophages (TAM) as major players of the cancer-related inflammation. *J Leukoc Biol*. 2009;86:1065-1073.

33. Yoshimura T. The production of monocyte chemoattractant protein-1 (MCP-1)/CCL2 in tumor microenvironments. *Cytokine*. 2017;98:71-78.
34. Harmsen AG, Muggenburg BA, Snipes MB, Bice DE. The role of macrophages in particle translocation from lungs to lymph nodes. *Science*. 1985;230:1277-1280.
35. Miserocchi G, Sancini G, Mantegazza F, Chiappino G. Translocation pathways for inhaled asbestos fibers. *Environ Health*. 2008;7:4.
36. NIOSH. Current Intelligence Bulletin 62. Asbestos Fibers and Other Elongate Mineral Particles: State of the Science and Road map for Research. 2011. <https://www.cdc.gov/niosh/docs/2011-159/pdfs/2011-159.pdf>. Accessed 24 Oct 2017. 2011.

SUPPORTING INFORMATION

Additional supporting information may be found online in the Supporting Information section at the end of the article.

How to cite this article: Abdelgied M, El-Gazzar AM, Alexander DB, et al. Potassium octatitanate fibers induce persistent lung and pleural injury and are possibly carcinogenic in male Fischer 344 rats. *Cancer Sci*. 2018;109:2164-2177. <https://doi.org/10.1111/cas.13643>